

UNIVERSITY OF CALIFORNIA
SANTA CRUZ

DISTRIBUTED BRAGG REFLECTOR ON ARROW WAVEGUIDES

A thesis submitted in partial satisfaction of the
requirements for the degree of

BACHELOR OF SCIENCE

in

PHYSICS

by

Raul A. Reyes Hueros

June 2018

The thesis of Raul A. Reyes Hueros
is approved:

Professor Robert P. Johnson, Chair

Professor Holger Schmidt

Professor David Smith

Copyright © by
Raul A. Reyes Hueros
2018

Abstract

Distributed Bragg Reflector on ARROW Waveguides

by

Raul A. Reyes Hueros

A new optofluidic chip design for an on-chip liquid dye laser based on Anti-Resonant Reflecting Optical Waveguides (ARROW) is developed. The microfluidic device is compact, user friendly and, most importantly, can provide the role of a on chip laser. This thesis can be broken into three parts: First, an analysis on distributive feed back (DFB) gratings that is developed to fabricate a optofluidic dye laser from anti-resonant reflecting optical waveguides (ARROW). Second, the reflection spectrum and plausible parameters for the proposed device are simulated with Roaurd's Method. Third, a technique for direct dry transfer of uniform poly (methyl methacrylate) (PMMA) is used to overcome the challenges encountered in conventional PMMA deposition on top of non-flat waveguide structures.

Table of Contents

Abstract	iii
List of Figures	vi
List of Tables	viii
Acknowledgments	ix
1 Introduction	1
1.1 Motivations for Building On-chip Bragg Reflector	2
1.2 Thesis Organization	3
2 Background	4
2.1 Distributed Bragg Reflector Gratings	4
2.2 Organic Dye Molecules	7
2.2.1 Population Inversion	7
2.3 Liquid Dye Laser	9
3 Anti-Resonant Reflecting Optical Waveguides	12
3.1 Theory	13
3.2 Loss	15
4 Design and Fabrication	17
4.1 Rouard's Method	17
4.1.1 Simulations	20
4.1.2 Summary	24
4.2 Fabrication Process and Complication	25
4.2.1 Summary	29
5 Future Directions	31
A Tables	32

B Simulation Code, Rouard's Method	33
Bibliography	37

List of Figures

2.1	Scattering of incident light on a thin layer with effective index n_2	5
2.2	Stack of dielectric material with varying effective index, n . A and B represent the traveling wave to the right and left respectively. The thickness of each dielectric material is shown as x_i	6
2.3	Energy levels for a typical organic dye with highlighted laser transition [18].	8
2.4	Simplified schematic of a Dye Laser. P-incoming pump laser, G-Gain Medium in the laser cavity, A-Birefringent filter, and O-Out going laser produced by the cavity [23].	10
3.1	Simple Schematic of hollow core waveguide intersection. A) in the y-x plane and B) in the y-z plane [29].	13
4.1	Dielectric slab surrounded by bounding media n_0 and n_1	18
4.2	Simplistic diagram of the DBR Structure with the gain medium in dark blue, mirror in the left and the gratings in gray with parameters: Λ is the period of the gratings, L is the total length of the DBR, n_1 and n_2 are the values of the varying effective index.	20
4.3	Values of effective index for increased etching depth as calculated by FIMMWAVE on SC-ARROW of total height = $12.2\mu\text{m}$ and core height = $6.7\mu\text{m}$	22
4.4	Reflection of a $L = 0.1\text{mm}$ Bragg grating for different Δn with $\Lambda = 198\text{nm}$ and first order ($m=1$).	23
4.5	Reflection of a Bragg gating with constant $\Delta n = 10^{-4}$ and varying length (L) with $\Lambda = 198\text{nm}$ and first order ($m=1$).	23
4.6	Simulated reflectivity spectrum of a first order structure with resonance at 599.97nm , this is also the common shape of these peaks.	24
4.7	Solid core waveguide of $2\mu\text{m}$ width that demonstrates the problem with the conventional method of spreading photoresist, PMMA.	26

4.8	Steps toward transfer of uniform PMMA film: A) A glass slide. B) Layer of Scotch tape and introduce PMMA. C) Spin and proceed with baking the structure for 3 min at 150°C. D) The PMMA is ready to be peeled. To facilitate the process, the desired area of PMMA is delineated. E) A frame made from Kapton tape is placed and compressed, via a flight edge, over desired area. F) The frame is gently peeled and the PMMA film is ready for use.	28
4.9	Application of PMMA film: A) Intersection of ARROW waveguide. B) Film of PMMA is introduced. C) The structure is baked at 150°C for 1 min. D) The film collapses and adheres over the waveguide.	28
4.10	PMMA patterning test on HC-ARROW when using Transparent Scotch Tape 4184, A) increased exposure from right to left. B) A close up on the three least exposed patterns, with a further enhancement on the right. C) Unknown layer that is peeled from the Transparent Scotch Tape 4184. D) Resulting patterning after three dummy peels, unknown layer is gone.	30

List of Tables

- A.1 Values from Rouard's Method using the following parameters: $\Delta n = 10^{-4}$, Bragg wavelength = 198nm and first order ($m=1$), the Length is varying. . . 32
- A.2 Values from Rouard's Method using the following parameters: Length (L) = 0.1mm , Bragg wavelength = 198nm and first order ($m=1$), Δn is varying. . . 32

Acknowledgments

I would like to thank my advisor, Dr. Holger Schmidt for giving me the opportunity to work under his guidance and for placing me with a patient mentor, Jennifer Black. I would also like to thank my mother, Soledad Hueros Soto, for her continues support and dedication towards my success. Without her I would't have been able to accomplish half of the achievements I've acquired. Finally, I want to thank my friends for the countless nights we've spent together.

Chapter 1

Introduction

Here we implement a new optofluidic chip design for an on-chip liquid dye laser that produces coherent monochromatic light. The optofluidics field can be characterized by the entanglement of two fields: microfluidics and photonics, the study of fluidic functionalities in the micron scale and the generation, regulation, and detection of photons, respectively. The optical properties of a dye laser [1] heavily rely on its liquid medium, which is commonly chosen to be an organic dye molecule. The recent developments in optofluidics [2-11] have transcended the integrations of nanostructures, hastening the progress of the Lab-on-Chip (LoC). The LoC is a device that combines full laboratory processes or functions into a miniaturized system, usually no bigger than a couple of squared centimeters. This growth is predominantly due to the advances that have happened in microfabrication over the past decade[12][13].

1.1 Motivations for Building On-chip Bragg Reflector

The advantages of a miniaturized system are transportability, reduction of required fluidic media or bioparticles sample, and the re-configurability of devices to have multiple means for analysis. This contributes to an overall reduction of device costs and, equally important, time for sample processing. We have reached the point where the technological advances have made the LoC components practical and reproducible. LoC devices will have an important impact on the world and on our ability to prevent epidemic outbreaks by making virus and bacterial detection an affordable investment for underdeveloped countries that wouldn't have the funds and infrastructure for the current biomedical devices.

Thanks to its multi-disciplinary research, optofluidics has been in the forefront of biomedical technology through its integrated LoC devices [14]. Cai et al. (2015) [15] recently reported the first vertically integrated device that combines established sample preparation techniques with single molecule optical detection. These types of optical experiments are based on fluorescence detection, which relies on light guiding for excitation, emission collection, and signal quality. The optofluidic device has integrated solid and liquid-core waveguides to meet this end. However, this requires tedious and time-consuming butt-coupling of optical fibers to the optofluidic platform. The next logical step would be to develop a compact on-chip laser that could be conveniently coupled to multiple integrated systems [15][16]. This is accomplished by replacing the discrete mirrors in the laser cavity with Distributed Bragg Reflectors (DBR) made from Anti-Resonant Reflecting Optical Waveguides (ARROW).

1.2 Thesis Organization

This thesis explores the possible implementation of Distributive Feed Back gratings on ARROWs to form an on-chip liquid dye laser. The structure is as follows: Chapter 2 contains the background needed to understand the basis of this thesis. This includes the components of the liquid dye laser and a successful LoC device. Chapter 3 presents the ARROWs and the need-to-know calculations for the loss in such waveguides. Chapter 4 describes the Rouard's method, theoretical calculations used to define the parameters of our device and the efforts to fabricate the device using new nanolithography techniques. Chapter 5 concludes with a description of the future work.

Chapter 2

Background

This chapter is broken down into five sections: Section 2.1, defines the properties of Distributed Bragg Reflector Gratings and a general perspective towards their configuration. Section 2.2, an attempt is made to breakdown a laser into digestible condense parts. Section 2.3, historical background on lasers and the transition towards liquid dye laser [18]. Section 2.4, reviews the general properties of organic dye molecules, including a physical description of light absorption and emission. Section 2.5, discusses a fully functional LoC and a microfluidic dye laser developed by distinct groups.

2.1 Distributed Bragg Reflector Gratings

DBR gratings can, essentially, be thought of as a thin-film stack of varying dielectric material. Let's first describe the general idea behind thin film theory and then mold it to fit our needs. When monochromatic light is incident to a surface it either transmits or reflects. There are three main variables that determine this effect: angle of incident (θ_1),

thickness of film (d) and effective index of the material (n). A second reflection can be produced by adding an extra layer, Figure 2.1.

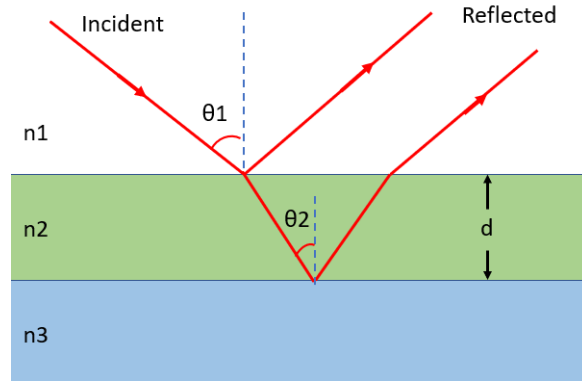


Figure 2.1: Scattering of incident light on a thin layer with effective index n_2 .

This second reflection now must travel an extra distance $2d\cos(\theta_2)$ to reach the first top layer. Once both reflected waves meet up, they combine to produce the resulting wave. This final wave could be amplified or destroyed depending on the phase acquired by the second reflection. Now let the incoming source of light have multiple wavelengths. Each wavelength will have a unique period and will therefore have different reflection and transmission conditions. By adding extra layers, we can take advantage of the phenomenon previously discussed. The final transmitted and reflected wavelengths can be picked by carefully tuning the parameters.

In principle, a stack of dielectric material with periodic changes in the refractive index is known as a DBR grating. Figure 2.2 demonstrates how the propagating waves A_o and B_o are reflected and transmitted through the stack.

In the case of Bragg reflectors, the dielectric medium is etched through micro-

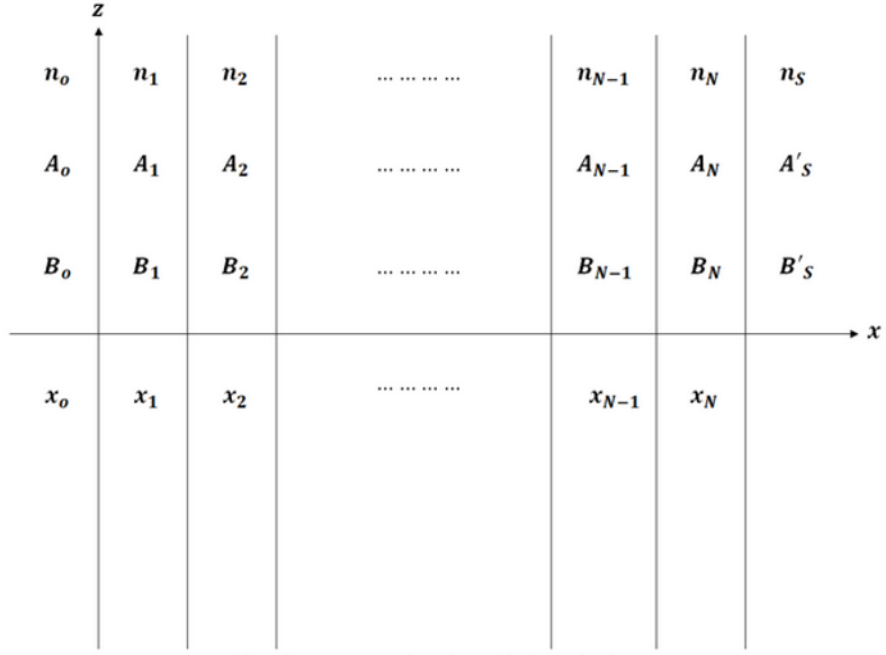


Figure 2.2: Stack of dielectric material with varying effective index, n . A and B represent the traveling wave to the right and left respectively. The thickness of each dielectric material is shown as x_i .

fabrication techniques, allowing air to replace some of the material. This decreases the effective index in the region x_i . Appendix A has an in-depth description of the Fresnel equations, Airy functions, and Maxwells equations that provide a quantitative description of the transmitted and reflected light. The frequency for maximum reflection created by these arrangements is controlled by the Bragg condition:

$$m\lambda = 2n\Lambda$$

where λ is the m th Bragg wavelength, n is the effective index and Λ is the grating period ($x_i + x_{i+1}$). Changing the grating period allows the structure to lase for a range of wavelengths. Due to the strong Bragg condition, the selected wavelength is allowed to lase while the

others are restricted and contribute to loss. This allows the dumping of a broad band of wavelengths (i.g. white light) to excite gain medium, making it easier to achieve the wanted wavelength. Carefully choosing these parameters for these gratings allows the DBR Reflector to be a mirror with wavelength selective properties.

2.2 Organic Dye Molecules

These dye molecules are complex and have a large number of spin and rotational states. The organic compounds that compose these dyes usually contain double bonds separated by a single bond. Alternating single and double carbon bonds ($=C-C=C-C=C-$) are a common chain for these molecules. The nature of these structures allows multiple vibrational and rotational energy levels, which broadens the absorption band. Having a wide absorption band allows the possibility of tuning in order to produce a narrow bandwidth along the desired emission. This property and its good quantum efficiency is the reason the dye laser is successful and overshadows its unfriendly aspects that will be discussed in Section 2.3.

2.2.1 Population Inversion

The selection rule states that the difference in total spin when transitioning to a different energy level must be zero, $\Delta S = 0$. This quantum mechanical phenomenon is essential to electromagnetic radiation and hence, lasers. Figure 2.3 shows the first few energy levels of a dye molecule, the rest are omitted for simplicity. Notice how there are two possible types of states: singlet and triplet. The singlet states are labeled as S_o and S_1 for

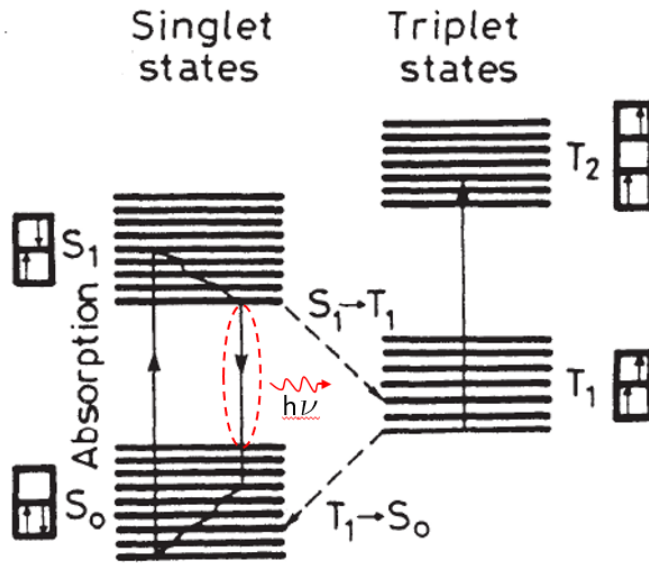


Figure 2.3: Energy levels for a typical organic dye with highlighted laser transition [18].

the ground state and first excited singlet states, similarly T_1 and T_2 for the triplet states. The characteristic difference of these types of states can be seen in the small boxes next to the energy levels. Notice how singlets always contain electrons with opposite spin which creates a total spin $S = 0$, satisfying the Pauli exclusion principle. In contrary, the triplets have electrons of the same spin and total spin $S = 1$. By the selection rule, transitions from singlet to triplets are not allowed. Figure 2.3 also shows how the main energy levels split into sublevels. This is due to the vibrational and rotational states that the molecule can occupy. Therefore, these complex structures have homogeneous broadened spectra that efficiently absorb and emit a narrow band [17].

Population inversion is accomplished by forcing the molecules into higher energy levels such that the occupied high energy states exceeds the population in the ground

state. Statistically, high energy levels are less likely to be occupied, but dye molecules have excited energy states with relatively long life time (nanoseconds). The external pump creates this inversion, which allows for an S_1 state to spontaneously drop to the ground state. This process emits a photon that forces stimulated emissions of other photons of the same wavelength, also known as lasing.

In practice, singlet to triplet states occur when the spin of an electron is flipped from collisions with other molecules, known as intersystem transitions [18]. A molecule could then transition from S_1 to T_1 , leaving the molecule with two possibilities: 1) transition to a higher triplet state by the absorption of the excitation or emitted light. 2) decay to the ground state (S_0) by interactions with its surroundings, a non fluorescent transition. Since the lifetime of the triplet state can range from microseconds to milliseconds [19], the dye molecule could be trapped in a state and denied the chance to lase. This can be avoided by pumping the dye molecules, since the triplet states are less common than singlets they aren't allowed the chance to build up. A more sophisticated method would be to introduce a birefringent filter as discussed in the following section.

2.3 Liquid Dye Laser

In 1960 T.H. Mainman created the first light amplification by stimulated emission of radiation (laser) by capitalizing on the theoretical work of Albert Einstein [20], on optical amplification by stimulated emission, done 44 years prior. Less than a decade later, there was an abundance of different laser subgroups: gas, chemical, solid-state and dye lasers. The remainder of this section will discuss the general components of the dye laser and the

goal of the device.

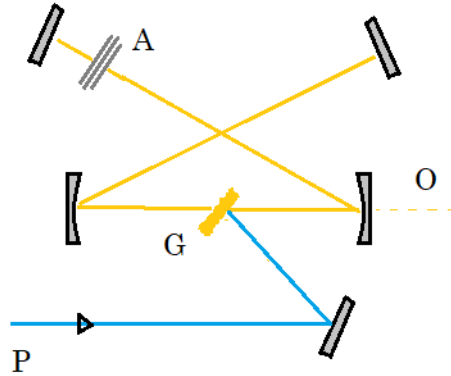


Figure 2.4: Simplified schematic of a Dye Laser. P-incoming pump laser, G-Gain Medium in the laser cavity, A-Birefringent filter, and O-Out going laser produced by the cavity [23].

The optical properties of a dye laser [1] heavily rely on its liquid medium, element G in Figure 2.4. An organic dye molecule (ODM), such as rhodamine 6G, is commonly used for the optical gain, and is selected depending on the required lasing wavelength and spatial mode. Section 2.2 attempts to characterize ODMs, but the reader is directed toward the numerous review articles for a detailed analysis on liquid mediums [21-25]. A dye laser depends on a high energy source (P) to excite the gain medium, allowing electrons in the dye molecules to jump towards a higher energy level where they experience stimulated emission or spontaneous emission. The lowest excitation level where the ratio is dominated by stimulated emission is known as the lasing threshold. There are various factors, including triplet-state absorption and pulse rate, that can make it difficult to reach the threshold. The light emitted is then allowed to propagate in the laser cavity. Photons can then continue to interact with the gain medium and increase the total amplitude. Mirrors are used to meet this end, theoretically there is a mirror (M1) with 100 % reflectivity and mirror (M2) with

80-90% reflectivity. This allows some of the propagating wave to escape the cavity and be used.

In practice the dye in the cavity is constantly flowing decreasing the time each molecule has in the cavity region. This is done to prevent triplet states and to assure the dye hasn't been saturated. Different dyes have different absorption and emission spectra. The frequency spacing between the spectral resonating modes of the dye laser can be controlled by varying the cavity length and index of the dye, also known as the free spectral range (FSR). This allows dye lasers to emit wavelengths that are difficult to reproduce by other devices and the ability to generate both continuous wavelengths and ultra-short pulses [26]. A birefringent filter (A) is used to saturate the effects of the triplet state by selectively tuning the optical spectrum at the highest gain for the singlet state and creating loss at other wavelengths. These dyes are often poisonous, odorous, and can also be combustible, giving the dye laser a reputation of not being user friendly. For this reason, they are only used in fields such as spectroscopy and photonics, where the large tunability and tough to generate wavelengths are essential.

Chapter 3

Anti-Resonant Reflecting Optical Waveguides

A conventional waveguide is based on total internal reflection; a core with a greater index of refraction than its surroundings. The issue with these waveguides occurs when a substance of a lower effective index than the surrounding cladding is introduced, forcing the light to propagate in the higher surrounding cladding. The anti-resonant reflecting optical waveguides (ARROWs) [27] overcome this issue by forming a Fabry-Perot reflector in the cladding layers with higher refractive indices than the core. This allows the longitudinal component of the light to continue to propagate throughout. Although ARROWs are leaky, and can be subject to high loss, they are valued for their low index guiding. This is essential for biosensing applications, a solutions with low effective index can be used as the core of the waveguide which, as mentioned, can't be accomplished with conventional waveguides.

3.1 Theory

The discussion of ARROWs will be divided into: solid core (SC-ARROW) and hollow core (HC-ARROW). Lets begin with the more complicated of the two, HC-ARROW. Since they both rely on the anti-resonant condition their discussion will be similar. A schematic of the structure can be seen in Figure 3.1. The core has an index of n_c with thickness d_c . For simplicity the surrounding cladding is shown as two layers, in our analysis this will be generalized to i layers with n_i index and d_i thickness respectively. Amnon Yarivs book Photonics: Optical Electronics in Modern Communications [28] and the discussion of ARROWs in J.Black's Thesis [29] is used for the remainder of this chapter.

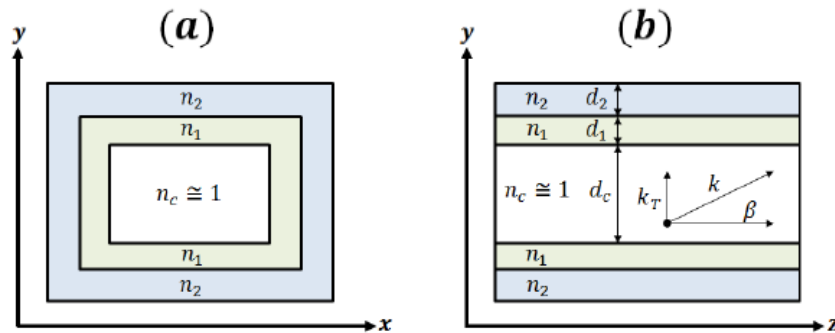


Figure 3.1: Simple Schematic of hollow core waveguide intersection. A) in the y-x plane and B) in the y-z plane [29].

The idea behind this method is, again, similar to a stack of thin films. The propagating vector k can be broken down into its transverse component, k_T , and its component along the z axis, β . These higher index layers, as mentioned earlier, are designed as Febyr-Pérot reflectors to allow propagation in the core. The modes that arise in an ARROW are transverse electric, TE, or transverse magnetic, TM. These depend on the polarization of the incident light, which changes the direction of the transverse modes. The anti-resonant

condition is based on forcing the round trip phase shift to be an odd multiple of π is and is as follows:

$$(2n - 1)\pi = 2d_i k_T + \phi_i \quad (3.1)$$

This is the condition for the i^{th} layer with n as a natural number representing the order and ϕ_i as the phase shift acquired by the bordering layers. Lets review the properties of the Brewster angle that will be key in determining ϕ_i .

$$\theta_B = \arctan\left(\frac{n_x}{n_i}\right) \begin{cases} n_x > n_i \text{ acquired phase shift: } \pi \\ n_x < n_i \text{ acquired phase shift: } 0 \end{cases} \quad (3.2)$$

The ϕ_i is then the addition of the phases acquired at each boundary. These conditions can then be implemented to the HC-ARROW as follows:

$$\begin{cases} n_c > n_1, \phi_i = \pi \\ n_{i+1} > n_i > n_{i-1}, \phi_i = \pi \\ n_i > n_{i+1}, n_{i-1}, \phi_i = 0 \end{cases}$$

By forcing the first layer in the ARROW to follow the middle condition, the phase shift acquired is obligated to be 0 or π making $2d_i k_t$ an odd multiple of π . It is possible to find the thickness of the i^{th} layer, d_i , from these constraints [30]:

$$d_i = \frac{N\lambda}{4\sqrt{1\left(\frac{n_c}{n_i}\right)^2 + \left(\frac{\lambda}{2t_c n_i}\right)^2}}, \quad N = \begin{cases} 1, 3, 5; \phi_i = 2\pi, 0 \\ 2, 4, 6; \phi_i = \pi \end{cases} \quad (3.3)$$

Were N is the number of anti-resonant layers, the rest of the variables have been assigned above. The SC-ARROW is based under the same principle, but only one side of the waveguide is forced to follow the anti-resonant condition. The core is commonly made

from SiO₂, this material has an effective index greater than one and the base has the layers of n_i and d_i that allow for the Fabry-Perot reflector. A silicon wafer, the base for these devices, has a large effective index and would compose the largest n_i . Since the core has an index larger than air, one, it guides via total internal reflection. SC and HC ARROWs are then able to be fabricated in the same silicon wafer.

3.2 Loss

Here we make no attempt on giving a thorough analysis of the theoretical loss in ARROW waveguides, instead the reader is directed towards P. Yehs Book, Optical waves in layered material [30]. This section also contains the results of a transverse matrix solved in Section 4.1 Rouards Method. The dynamic matrix for the multilayered system of dielectric material that composes the anti-resonant layers can be calculated by considering the continuity of electric fields at the boundaries. In essence, it becomes a convoluted boundary problem that can be cleverly managed by basic linear algebra techniques. The loss is then calculated by:

$$\alpha = \frac{(1 - R_1 R_2)}{2d_c \tan(\theta) \sqrt{R_1 R_2}} \quad (3.4)$$

Here d_c is the cores width, θ is the angle of incidence from the core to the dielectric slabs and R_i is the reflectivity of the i^{th} slab. The theoretical loss of both x-y polarized TE and TM modes can now be calculated. In reality, the waveguides have imperfections that are currently unavoidable in the fabrication process and create higher loss than the theory presumes. The minimum loss from TE and TM modes can be calculated as follows:

$$\begin{aligned}
\alpha_{Min.TE} &= \left(\frac{n_2^2 n_c^2}{n_1^2 n_c^2} \right)^{N/2} \alpha_o \\
\alpha_{Min.TM} &= \left(\frac{n_1^{N+1}}{n_1 n_c^N} \right)^2 \alpha_{Min.TE} \\
\alpha_o &= \frac{\lambda^2 m^2}{n_c d_c^3 \sqrt{n_1^2 n_c^2}}
\end{aligned} \tag{3.5}$$

where N represents the number of anti-resonant layers and m is the mode order, a positive integer. These minimal loss equations give a threshold that becomes important when designing the ARROW waveguides.

Chapter 4

Design and Fabrication

4.1 Rouard's Method

The Rouard's method for waveguide gratings is based on the Weller-Brophy paper [32]. The Rouard's Method is used to analyze how two opposite propagating plane waves transmit through the periodic or non-periodic gratings, which simplifies our structure by treating it as periodic dielectric slabs stacked on top of each other. Think about each total effective index of each structure being stacked, to solve for the transmission and reflection. One of the great aspects of this method is that it lends itself to graphs and visual representations, making it easier to analyze and justify the result.

We will start with the simple case of just one dielectric slab, and then generalize the process. The incoming electric field can be written as:

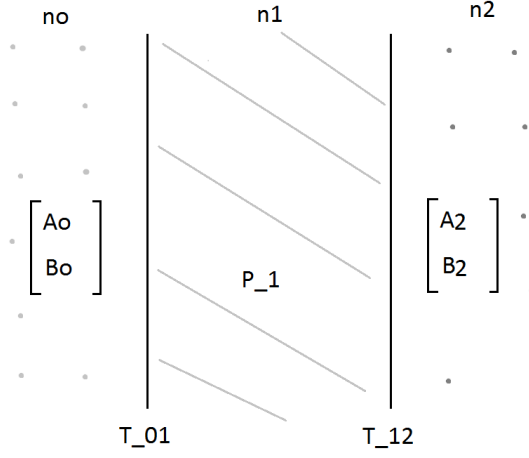


Figure 4.1: Dielectric slab surrounded by bounding media n_0 and n_1 .

$$\begin{cases} (A_0 e^{-\beta_0 y} + B_0 e^{\beta_0 y}) e^{-i h y}, & \text{medium1} \\ (A_1 e^{-\beta_1 y} + B_1 e^{\beta_1 y}) e^{-i h y}, & \text{medium2} \end{cases} \quad (4.1)$$

where A_0 and A_1 are the amplitudes of right traveling waves (+y), while B_0 and B_1 are left traveling (-y), and we are assuming normal incidence. The β and h in these equations are the same as the ones in 2.1. These waves propagate until they encounter the dielectric slab. At this point some of the wave is reflected and transmitted; this is known as the transition matrix T .

$$T_{0,1} = \frac{1}{2n_0} \begin{bmatrix} n_0 + n_1 & n_0 - n_1 \\ n_0 - n_1 & n_0 + n_1 \end{bmatrix}$$

The part of the wave that passes through then propagates through the new media. This is the step where the wave catches a phase shift and its described by P , the propagation matrix.

$$P = \begin{bmatrix} e^{i\beta d} & 0 \\ 0 & e^{-i\beta d} \end{bmatrix}$$

Finally, the wave interacts with the end of the dielectric slab by another transition matrix and then continues to propagate through the last medium. This process needs to be done in the right order since matrices don't commute.

$$\begin{bmatrix} A_o \\ B_o \end{bmatrix} = T_{0,1} P_1 T_{1,2} \begin{bmatrix} A_2 \\ B_2 \end{bmatrix}$$

Figure 4.1 shows the schematic of Rouard's method. Imagine that now we have stacked up N layers of these dielectric slabs, the process would be the same, it would just involve more matrices.

$$\begin{bmatrix} A_o \\ B_o \end{bmatrix} = T_{0,1} P_1 T_{1,2} P_2 T_{2,3} \dots T_{N-1,N} P_N T_{N,N+1} \begin{bmatrix} A_{N+1} \\ B_{N+1} \end{bmatrix} = \begin{bmatrix} M_{11} & M_{12} \\ M_{21} & M_{22} \end{bmatrix} \begin{bmatrix} A_{N+1} \\ B_{N+1} \end{bmatrix}$$

$$\begin{bmatrix} M_{11} & M_{12} \\ M_{21} & M_{22} \end{bmatrix} \begin{bmatrix} A_{N+1} \\ B_{N+1} \end{bmatrix} = M \begin{bmatrix} A_{N+1} \\ B_{N+1} \end{bmatrix}$$

Where the 2x2 M matrix holds the information of the total transmitted and reflected wave:

Total Transmitted = $\frac{1}{M_{11}}$ and Total Reflected = $\frac{M_{21}}{M_{11}}$. As mentioned earlier, the Rouard's

method allows us to model more complicated structures more easily (e.g. adding defects, varying Bragg spacing, or any variation which breaks the periodicity of the grating), that are not possible by coupled-mode theory.

4.1.1 Simulations

The application of the Rouard's method is straightforward and can be implemented with a few lines of code; Appendix B contains the bare bone Python code. Figure 4.2 shows the DBR device with the parameters that can be manipulated in our simulations: Λ is the period of the gratings and can be calculated from the Bragg condition, L is the total length of the DBR, while n_1 and n_2 are the values of the varying effective index. For this design the laser cavity is composed of an ideal mirror on the left and a DBR on a SC-ARROW on the right, acting as the output mirror. A pump laser is used to excite the organic dye molecules by pumping the gain from above. The construct is different, but it is theoretically the same as a full scale liquid dye laser. Since the ARROW waveguide uses multiple layers to create its anti-resonant condition it is difficult to derive the characteristic equations for the effective index of the structure. For this reason it is common to use a mode solver for 3D waveguide structures, such as FIMMWAVE, to solve the effective index n_1 and n_2 . All index values in this paper have been calculated using FIMMWAVE.

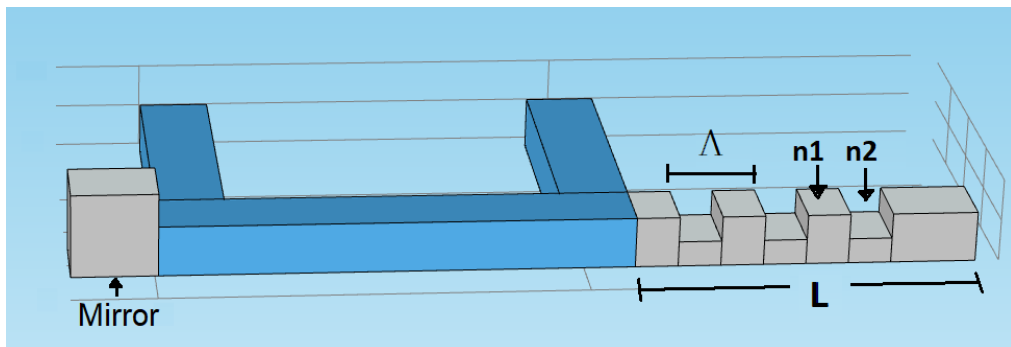


Figure 4.2: Simplistic diagram of the DBR Structure with the gain medium in dark blue, mirror in the left and the gratings in gray with parameters: Λ is the period of the gratings, L is the total length of the DBR, n_1 and n_2 are the values of the varying effective index.

The constraints of these parameters emerge from the limitations in the fabrication

process. The following discussion will focus on the limitations brought forth by the scanning electron microscope (SEM) that is used to perform e-beam lithography. The SEM sends a focused beam of electrons to an electron-sensitive film; in this case the layer is made of poly(methyl methacrylate) (PMMA), to expose the layer and create custom patterning. There are two main constraints with SEM: 1) The focused beam of electrons has a couple of millimeters of area that it can operate on and would have to be refocused to operate outside this range. Refocusing is an issue because it could expose the PMMA to the beam. This process could be done in the dark, with the e-beam turned off, but requires careful precision and is best avoided. 2) The smallest Λ value is dependent on the precision of the SEM and the thickness of the PMMA. A good rule of thumb is that the size of the grating should be roughly around the thickness of the PMMA. The technique used in the following section allows a PMMA thickness of 200nm or more. A dedicated e-beam writer and high quality photoresist would allow for narrower gratings.

The SC-ARROW was studied in detail with FIMMWAVE in order to home in on possible ranges for Δn , the difference between n_1 and n_2 . Figure 4.4 shows how the effective index changes as the top layers in the waveguide are removed. The orange line represents the Δn (10^{-4}) right before the low index oxide in the core is reached (please refer to Section 3.1) while the green line illustrates the Δn (10^{-3}) commonly used in these types of devices [33]. The core is where the mode propagates; if this portion is etched then the mode is deformed and could create loss. This could be thought of as fluid flowing through a pipe; if the pipe is suddenly expanded and contracted the fluid will fill these new gaps and the flow will be disrupted. This analogy works as long as its not taken literally.

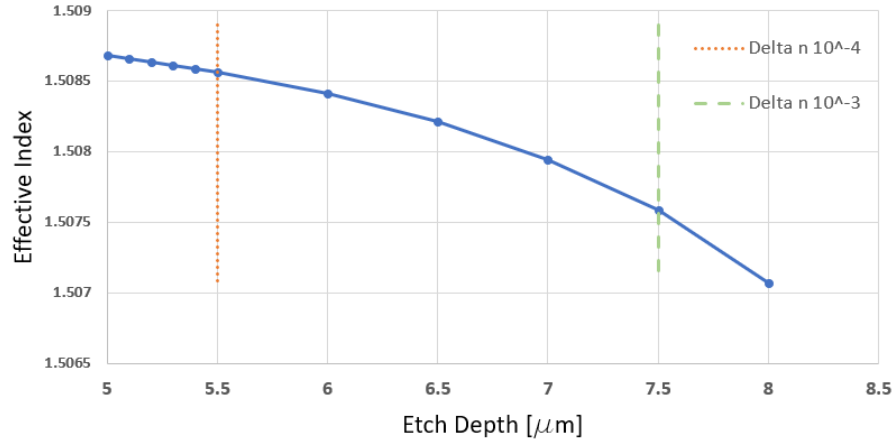


Figure 4.3: Values of effective index for increased etching depth as calculated by FIMMWAVE on SC-ARROW of total height = $12.2\mu\text{m}$ and core height = $6.7\mu\text{m}$.

Figure 4.4 uses the Rouard's method to calculate the reflectivity from the DBR with varying Δn and optimal grating length, $L = 0.1\text{mm}$. Similarly, Figure 4.5 has varying L and Δn is fixed as if etched to just above the core. It seems that the reflection will not be able to reach the 80%-90% that would be ideal for a output mirror, without deviating from the ideal values. The length is the parameter that will have to vary from the set ideal, since creating a larger Δn would create problems with the confinement of power.

The gain spectrum for Rhodamine 6G, the intended gain, spans 550nm to 650nm. The gain medium dictates the spectrum where the dye laser is allowed to lase. This is accounted for with the Bragg condition by letting $\lambda = 600\text{nm}$. Figure 4.6 shows an example of the simulated reflectance spectrum for the DBR structure with the parameters: $n_1 = 1.5086$, $n_2 = 1.5075$, hence $\Delta n = 10^{-4}$, $\Lambda = 198\text{nm}$ and $L = 3\text{mm}$. Notice that these values all still fall under plausible values discussed above.

First order DBR structures are widely used for their ability to achieve low thresh-

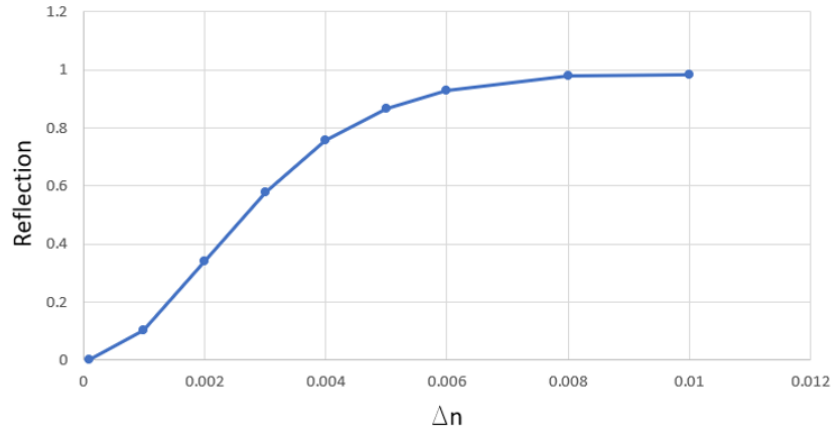


Figure 4.4: Reflection of a $L = 0.1\text{mm}$ Bragg grating for different Δn with $\Lambda = 198\text{nm}$ and first order ($m=1$).

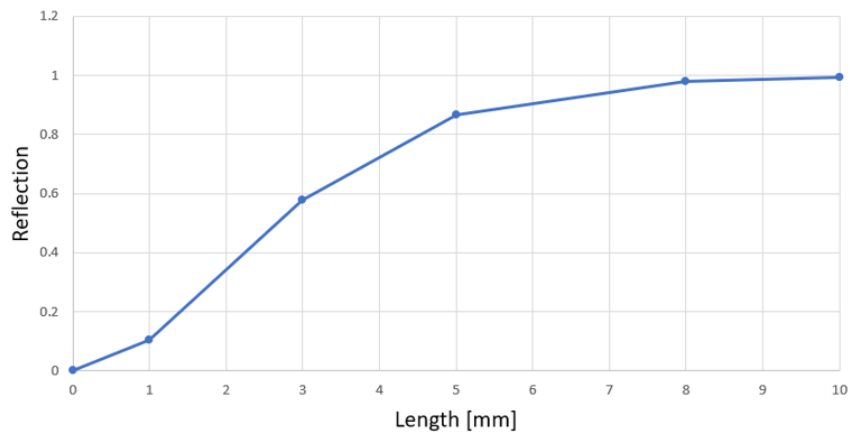


Figure 4.5: Reflection of a Bragg grating with constant $\Delta n = 10^{-4}$ and varying length (L) with $\Lambda = 198\text{nm}$ and first order ($m=1$).

olds and high efficiency, although higher order gratings are capable of multiple resonance that could be used to cover a wider range of the spectrum [33]. Increasing the order comes at a cost because the order is inversely proportional to the coupling coefficient [34]. The Bragg order is a parameter that must be taken into consideration when deciding the exact parameters for the DBR structure.

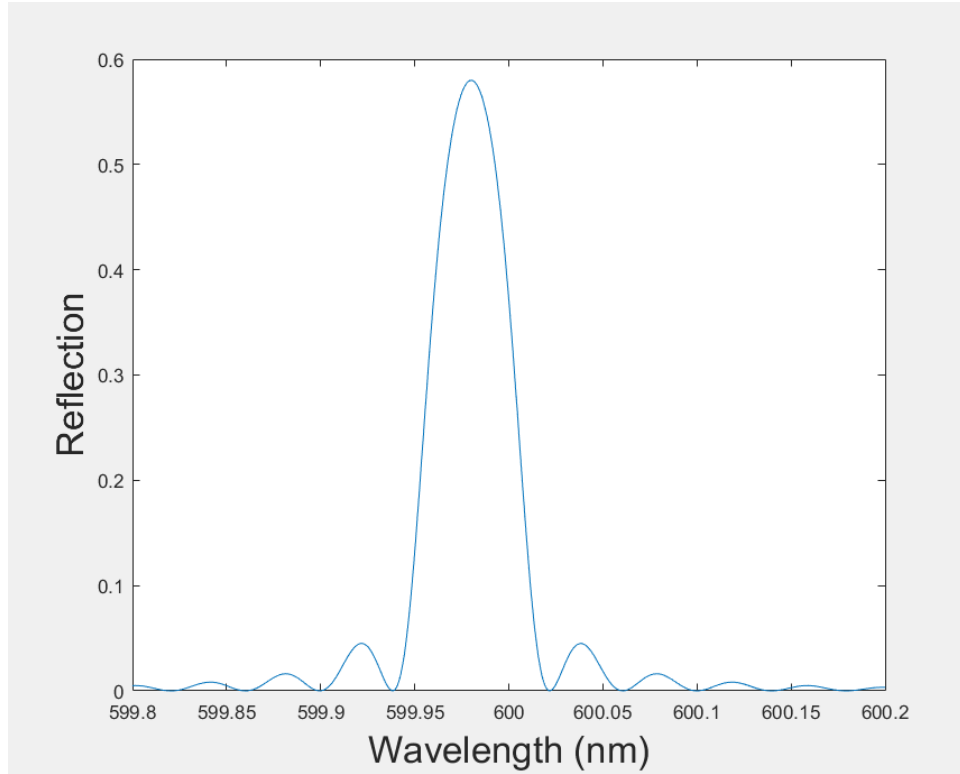


Figure 4.6: Simulated reflectivity spectrum of a first order structure with resonance at 599.97nm, this is also the common shape of these peaks.

4.1.2 Summary

In this section, we have proposed a novel DBR structure for a optofluidic dye laser. The simulations clearly demonstrate how reasonable reflection, greater than 40%, can be achieved with the predominant constraints of fabrication: $\Lambda \geq 100\text{nm}$, $\Delta n = 10^{-4}$ and $L \leq 8\text{mm}$. The $\Delta n = 10^{-4}$ can be achieved in the SC-ARROW without etching the low index oxide where the mode propagates. This keeps the mode constrained and reduces the loss. The reflection could further be improved by pushing the limits of the SEM, hence increasing the length (L) of the DBR structure. The theoretical DBR structure has other applications besides the one discussed here, such as biosensors and ultrashort pulse generators [35][36].

4.2 Fabrication Process and Complication

Our lab is able to fabricate SC-ARROWS and HC-ARROWS with minimal loss over reasonable distances [37]. This section will therefore focus on the fabrication of the DBR gratings on ARROWS. The general approach used when preparing a device for e-beam lithography involves spin coating a uniform layer of PMMA over the surface. Having an evenly distributed layer is an essential requirement, if not met the SEM can't accurately focus over the desired area. This method works great for large flat surfaces, but fails on irregular surfaces and small features [38][39]. The width of the ARROWS developed in our lab range from $5\mu\text{m}$ - $12\mu\text{m}$, but even more problematic is the abrupt change in height which is enough to cause problems such as those seen in Figure 4.7. Note, this is a simple solid core waveguide with width of $2\mu\text{m}$. The PMMA that was spin coated can only be seen on the pedestal and not on the top of the waveguide. This is made obvious by exposing a strip of the PMMA.

Special techniques have been developed to solve this problem. These include spray coating [40], photoresist (PR) evaporation [41], and dryfilm PR [42]. These methods require special equipment, lower exposure sensitivity and expensive materials respectively. Instead, a simpler method is pursued [43] [44], that allows for direct dry transfer of uniform PMMA films onto the substrate of interest. Figure 4.8 shows the main steps of this process that begin with, Figure 4.8 (A-B), the adhesion of Transparent Scotch[®] tape (seen in light gray) to a clean slide of glass. Unfortunately there are multiple recipes of Transparent Scotch[®] tape that could cause confusion, this is discussed later in the section. A flat edge, smooth enough such that it doesn't scratch the tape, can be used to ensure no air pockets are

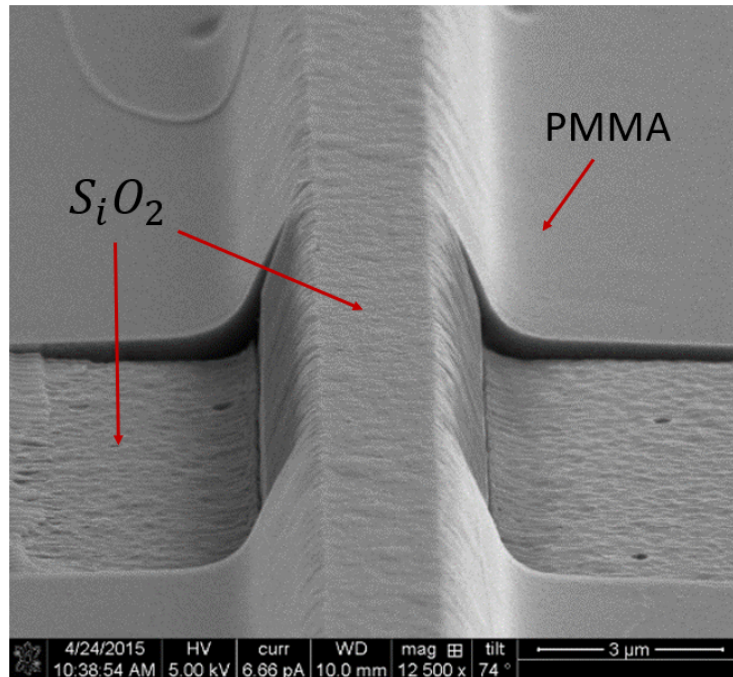


Figure 4.7: Solid core waveguide of $2\mu\text{m}$ width that demonstrates the problem with the conventional method of spreading photoresist, PMMA.

created. This layer of tape, unlike the glass, hardly adheres to the PMMA, allowing the PMMA to be peeled later on. Now PMMA is dropped over the tape. In Figure 4.8 (C) the slide is spun at 5,000rpm for 45sec and then immediately baked for 3min at 150C° . The spin rate depends on the type of PMMA which is usually diluted in some type of solvent. In this study PMMA 950 A5 is used, the dilution is expressed in percent solids dissolved in anisole; thus "A5" is a 5% dilution of PMMA in anisole. It is important to immediately bake the slide; the solvent can interact with the tape and potentially ruin the surface. Next, Figure 4.8 (D-E), the PMMA is ready to be peeled and to facilitate the process, the desired area of PMMA is delineated. There is no need to cut all the way through the tape, just enough to slice the thin PMMA layer. A Kapton[®] tape (seen in orange) is used as the frame. The frame is easily created by placing the Kapton[®] on a glass slide, the window is then simply

cut out via razor blade. A double sided Kapton[®] tape is firm, but it's this rigidity that creates a problem in the peeling process. For this reason, the single sided Kapton[®] tape is recommended, which allows the frame to bend with the PMMA film and prevent tearing. Lastly, Figure 4.8 (F), the frame is gently peeled and the PMMA film is ready for use.

The suspended PMMA is now ready to be transferred to the ARROW. The frame is gently placed over the waveguide, Figure 4.9 (A-D). The structure is then baked for 1min at 150°C to allow the PMMA to collapse and mold into the shape of the waveguide. The baking time and temperature can be improved to allow a complete collapse. In the original paper [43] the Kapton[®] frame was then removed while the PMMA is left on the device. This step is unnecessary for our purposes and the frame could also be used to remove the remaining PMMA after the etching is complete.

The remainder of this section is dedicated to the results and complications of the discussed process. A HC-ARROW of 10 μ m width and 5 μ m height was used as the test structure. A series of gratings was created in order to develop the appropriate recipe. Figure 4.10 A) demonstrates the full series of patterns of increasing exposure from right to left. Figure 4.10 B), the array is enhanced to show the repeating pattern composed of various openings (1 μ m, 200nm and 100nm) and spacing (3 μ m, 2 μ m, 1 μ m, 800nm, 600nm, 400nm, 200nm and 100nm). It is clear that the suspended PMMA can cause enough tension to create tears in the film. Not much attention is paid to this issue. Since our goal is to etch into the waveguide, what happens in the surroundings is of little importance. Our focus is instead directed toward Figure 4.10 C), where it becomes apparent that an unknown layer is being peeled from the Transparent Scotch[®] Tape 4184. The waveguide is not visible even

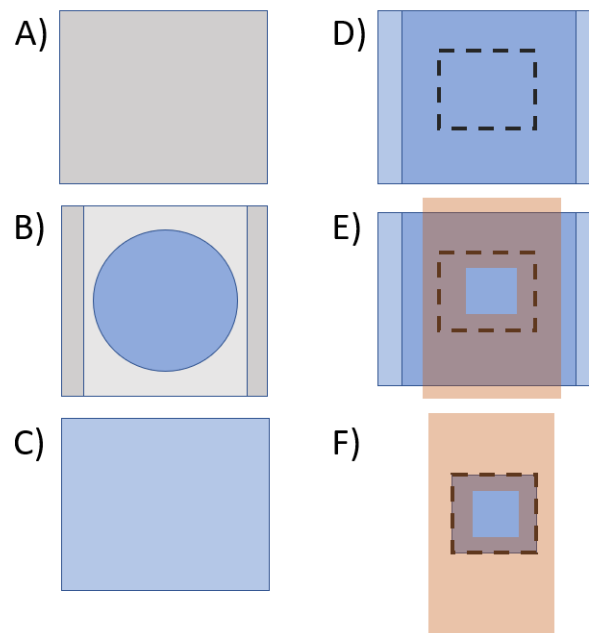


Figure 4.8: Steps toward transfer of uniform PMMA film: A) A glass slide. B) Layer of Scotch tape and introduce PMMA. C) Spin and proceed with baking the structure for 3 min at 150°C. D) The PMMA is ready to be peeled. To facilitate the process, the desired area of PMMA is delineated. E) A frame made from Kapton tape is placed and compressed, via a flight edge, over desired area. F) The frame is gently peeled and the PMMA film is ready for use.

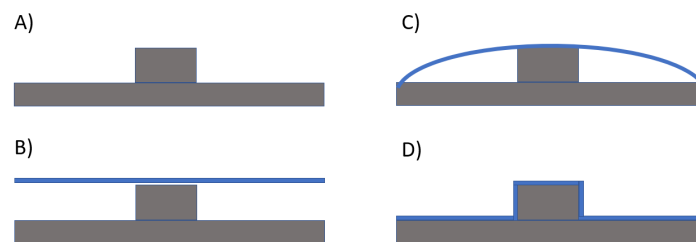


Figure 4.9: Application of PMMA film: A) Intersection of ARROW waveguide. B) Film of PMMA is introduced. C) The structure is baked at 150°C for 1 min. D) The film collapses and adheres over the waveguide.

when the gratings have lifted off, as seen in the enlarged image on the right. The process of creating the uniform peel is performed various times in an attempt to remove this unknown

layer. This is done while using the same layer of scotch tape (Figure 4.8 B-D)). The results are seen in Figure 4.10 D), where three dummy peels were used to fully remove the unknown layer. The PMMA forming the gratings seems to arc over the waveguide creating an uneven surface, an undesired factor, and could be avoided by retaining the pattern to just the top of the waveguide. Similar tests were conducted with transparent Scotch[®] Tape 600, a different recipe. A unknown layer was visible but the thickness of it was substantially less.

4.2.1 Summary

We have demonstrated a simple method for dry PMMA deposition onto irregular substrates [43] [44]. Hence, the fabrication of DBR on SC-ARROWs and HC-ARROWs is plausible. The patterning of PMMA achieved could be further improved by tuning the exposure time and appropriately picking the size of the gratings to match the waveguide's width. This would reduce the tension on the suspended PMMA and, as a result, reduce the tears in the film.

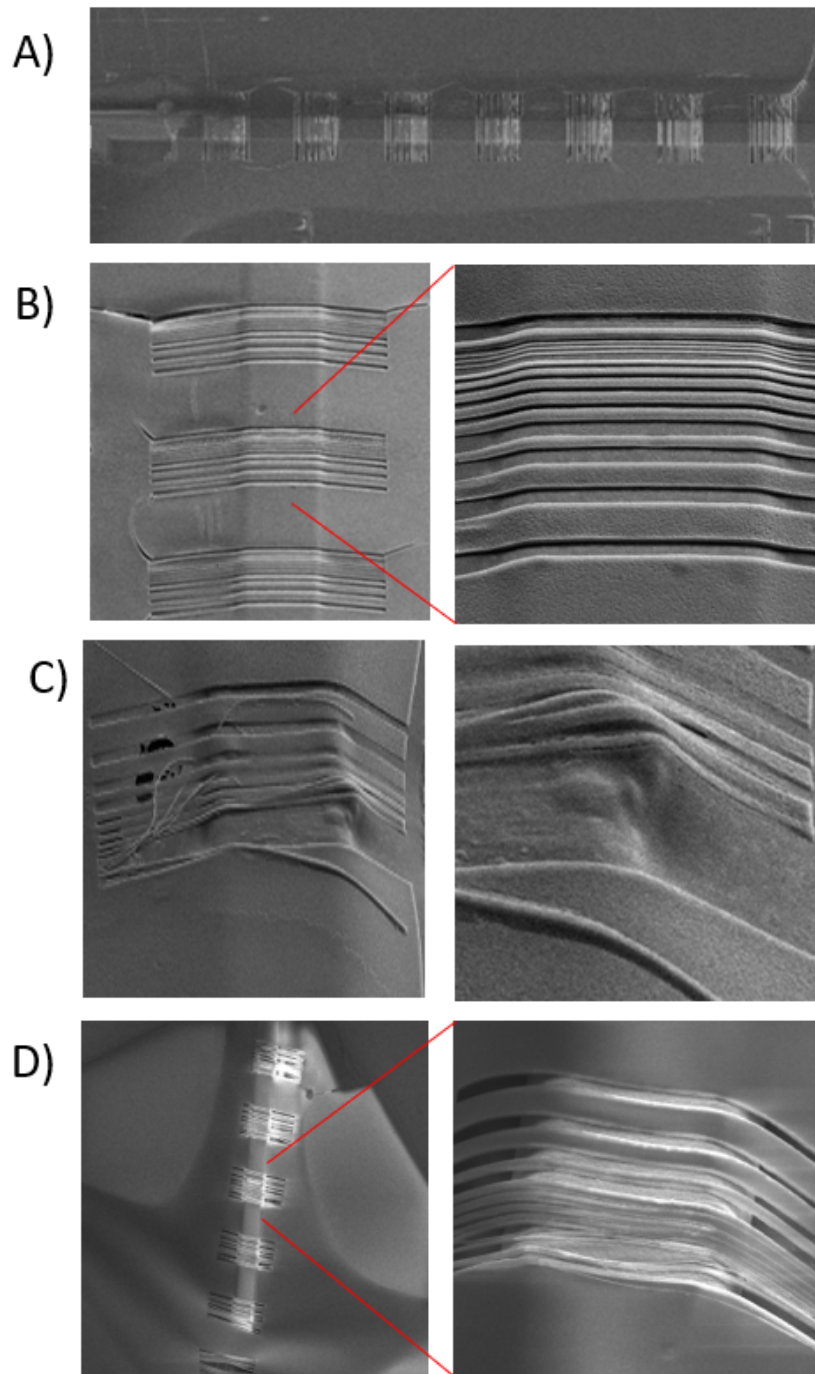


Figure 4.10: PMMA patterning test on HC-ARROW when using Transparent Scotch Tape 4184, A) increased exposure from right to left. B) A close up on the three least exposed patterns, with a further enhancement on the right. C) Unknown layer that is peeled from the Transparent Scotch Tape 4184. D) Resulting patterning after three dummy peels, unknown layer is gone.

Chapter 5

Future Directions

Here we have presented the necessary theoretical framework and fabrication techniques to build a optofluidic dye laser on ARROWs. The subsequent steps would include the deposition or etching of the ARROW and refinement of parameters for DFB. Although there have been great improvements, the optofluidic dye laser is in the early stages. It still falls under the performance of conventional dye lasers [45]. If this bar is met and the geometric and fluidic confinement limitations are dealt with, the lab-on-chip field will flourish. To the best of our knowledge, the optofluidic dye laser has not been incorporated to a full lab-on-chip system. This is a clear next step, but without an on-chip pump source the utility of the device will suffer.

Appendix A

Tables

L[mm]	Reflection
0.01	0.0013
1	0.1041
3	0.5790
5	0.8668
8	0.9808
10	0.9949

Table A.1: Values from Rouard's Method using the following parameters: $\Delta n = 10^{-4}$, Bragg wavelength = 198nm and first order ($m=1$), the Length is varying.

Δn	Reflection
0.0001	0.0013
0.001	0.1026
0.002	0.3389
0.003	0.5795
0.004	0.7566
0.005	0.8669
0.006	0.92939
0.008	0.98096
0.01	0.9843

Table A.2: Values from Rouard's Method using the following parameters: Length (L) = 0.1mm , Bragg wavelength = 198nm and first order ($m=1$), Δn is varying.

Appendix B

Simulation Code, Rouard's Method

```
# A 2x2 Matrix Multiplication
```

```
def Mult(A,B):\
```

```
C = np.zeros((2 , 2), dtype=np.complex)
```

```
C[0,0] = A[0,0]*B[0,0] + A[0,1]*B[1,0]
```

```
C[1,0] = A[1,0]*B[0,0] + A[1,1]*B[1,0]
```

```
C[0,1] = A[0,0]*B[0,1] + A[0,1]*B[1,1]
```

```
C[1,1] = A[1,0]*B[0,1] + A[1,1]*B[1,1]
```

```
return C
```

```
#Transition and Propagation Matrix
```

```
def TP(n1, n2, Beta1, Beta2, d):
```

```
T = np.zeros((2 , 2), dtype=np.complex_) #Transmission Matrix
```

```
P = np.zeros((2, 2), dtype=np.complex_) #Propagation Matrix
```

```
# Filling Matrices with initial values
```

```
T[0,0] = n1 + n2
```

```
T[0,1] = n1 - n2
```

```
T[1,0] = n1 - n2
```

```
T[1,1] = n1 + n2
```

```
P[0,0] = e**(1j*Beta2*d)
```

```
P[0,1] = 0
```

```
P[1,0] = 0
```

```
P[1,1] = e**(-1j*Beta2*d)
```

```
return T/(n1*2), P
```

```
#Multiplying the Transition and Propagation Matrices
```

```
in sequence. [4.9–25] Yariv 6th
```

```
def Transmision(n1, n2, Beta1, Beta2, wavelength, d,
```

```
                Grating_number):
```

```
    count = 0
```

```
    M = []
```

```
    M_matrix = 1
```

```
        while count <= (Grating_number + 1):
```

"""Appends the matrices (found in [4.9–25] Photonics
 Yariv, 6th Edition) to M. The order of these matrix
 multiplication matters."""

T = []

P = []

if count % 2 == 0: *#If even (2,4...)*

 T,P = T.P(n1, n2, Beta1, Beta2, d)

 M.append(T)

 M.append(P)

else: *#If odd (1,3...)*

 T,P = T.P(n2, n1, Beta2, Beta1, d)

 M.append(T)

 M.append(P)

 count += 1

first = M[0]

for i **in** M[1:]: *#Does the Matrix Mult in the correct order*

 hold = Mult(first, i)

 first = hold

M_matrix = first

return M_matrix

#-----TEST-----

```

y = []

wavelength_values = np.linspace(504.35*10**-9,704.45*10**-9,1000)

n1 = 1.3357

n2 = 1.3354

for wavelength in wavelength_values:

    Beta1 = n1 * (2*np.pi) / wavelength

    Beta2 = n2 * (2*np.pi) / wavelength

    Final_M = Transmission(n1, n2, Beta1, Beta2, wavelength, d,
                           Grating_number)

    to = 1 / Final_M[0,0]

    t = ((to)*(to.conjugate())) . real

    y.append(t)

plt.rcParams['figure.figsize'] = (9,7)

plt.plot(wavelength_values*10**9, y, '.g')

plt.ylim(0,1.1)

plt.show()

```

Bibliography

- [1] Schäfer, Fritz, et al., Organic Dye Solution Laser, Applied Physics Letters, Volume 9, Issue 8, p.306-309 (1966).
- [2] Monat, C., Domachuk, P. & Eggleton, B. J., "Integrated optofluidics: A new river of light". Nat. Photonics 1, 106114 (2007).
- [3] Schmidt, H. & Hawkins, A. R. "The photonic integration of non-solid media using optofluidics". Nat. Photonics 5, 598604 (2011).
- [4] Li, Z. & Psaltis, D. "Optofluidic Distributed Feedback Dye Lasers". IEEE J. Sel. Top. Quantum Electron. 13, 185193 (2007).
- [5] Tang, S. et al. "A multi-color fast-switching microfluidic droplet dye laser". Lab Chip 9, 2767 (2009).
- [6] Song, W. & Psaltis, D., "Pneumatically tunable optofluidic dye laser". Appl. Phys. Lett. 96, 35 (2010).
- [7] Bakal, A., Vannahme, C., Kristensen, A. & Levy, U., "Tunable on chip optofluidic laser". Appl. Phys. Lett. 107,211105 (2015).

- [8] Erickson, D., Rockwood, T., Emery, T., Scherer, A. & Psaltis, D., "Nanofluidic tuning of photonic crystal circuits". *Opt. Lett.* 31, 5961 (2006).
- [9] Bedoya, A. C. et al. "Reconfigurable photonic crystal waveguides created by selective liquid infiltration". *Opt. Express* 20, 1104611056 (2012).
- [10] Cuennet, J. G., Vasdekis, A. E. & Psaltis, D., "Optofluidic-tunable color filters and spectroscopy based on liquid-crystal microflows". *Lab Chip* 13, 27216 (2013).
- [11] Ozcelik, D. et al. "Dual-core optofluidic chip for independent particle detection and tunable spectral filtering". *Lab Chip* 12, 372833 (2012).
- [12] Fu, M.W.; Chan, W.L. (2013). "A review on the state-of-the-art microforming technologies". *International Journal of Advanced Manufacturing Technology.* 67 (9): 24112437
- [13] Xia, Y. N. and Whitesides, G. M., *Soft lithography. Annual Review of Materials Science*, 28:153184, 1998.
- [14] Ozcelik, D., Cai, H., Leake, K.D., Hawkins, A.R., and Schmidt, H., "Optofluidic bioanalysis: Fundamentals and applications", *Nanophotonics*, doi.org/10.1515/nanoph-2016-0156 (2017).
- [15] Parks, J.W., Cai, H., Zempoaltecatl, L., Yuzvinsky, T.D., Leake, K., Hawkins, A.R., and Schmidt, H., "Hybrid optofluidic integration", *Lab on a Chip*, 13, 4118 (2013).
- [16] Balslev S. et al., *Lab-on-a-chip with integrated optical transducers*, *Lab Chip*, 6, 213-217. (2006).

- [17] Jr Johnston T. F. "Tunable dye lasers", in Encyclopedia of physical science and technology, Meyers, Robert A. eds. Academic Press, Orlando, 1987.
- [18] Svelto O., "Principles of Lasers". Plenum Press, 1998.
- [19] Helbo, B., Kristensen, A. and Menon, A., "A Micro-Cavity Fluidic Dye Laser.J. Micromech. Microeng". PACS numbers: 42.55.Mv, 42.60. (2003)
- [20] Einstein A., "Erklärung der Perihelionbewegung der Merkur aus der allgemeinen Relativitätstheorie, Sitzungsber".(German) preuss.Akad. Wiss., vol. 47, No.2, pp. 831-839.(1915)
- [21] Sorokin, P.P., Moruzzi, VL., Hammond, E.C., Flashlamp-pumped organic-dye lasers. J Chem Phys 48(10): 47264741 (1968).
- [22] Snavely, B.B., Flashlamp-excited organic dye lasers. Proc IEEE 57(8):13741390 (1969).
- [23] Shank, C.V., Physics of dye lasers. Rev Mod Phys 47(3):649657 (1975).
- [24] Peterson, O.G., Dye lasers, Methods of Experimental Physics, vol 15A. Academic, New York, pp 251359 (1979).
- [25] Johnston Jr, T.F., Tunable dye lasers, Encyclopedia of Physical Science and Technology, vol14. Academic, New York, pp 96141 (1987).
- [26] Li, Z., et al., "Single mode optofluidic distributed feedback dye laser." Optics Express 14.2: 696-701 (2006).
- [27] Yin, D., Schmidt, H., Barber, J.P., and Hawkins, A.R., "Integrated ARROW waveguides with hollow cores", Optics Express Vol. 12, Issue 12, pp. 2710-2715 (2004)

- [28] Yariv, Amnon, and Yeh P., "Optical electronics in modern communications", Photonics, Vol. 6. New York: oxford university press, 2007.
- [29] Black, J., "Atomic Cooling via AC Stark Shift", University of California Santa Cruz, Santa Cruz, CA.(2014)
- [30] Duguay, M. A., Kokubun, Y., Koch, T. L., and Pfeiffer, L., Antiresonant reflecting optical waveguides in SiO₂Si multilayer structures, Appl. Phys. Lett., vol. 49, no. 1, pp. 1315, Jul. 1986.
- [31] Yeh, P., "Optical waves in layered material". Wiley-Interscience, 2005.
- [32] Weller-Brophy, L. A., and Hall, D. G., Analysis of waveguide gratings: application of Rouards method. JOSA A 2.6 (1985): 863-871.
- [33] Zhenyu, Li., et al. (2006), "Single mode optofluidic distributed feedback dye laser." Optics Express 14.2: 696-701.
- [34] Streifer, W., Scifres, D. R., and Burnham, R. D., "Coupling coefficients for distributed feedback single-heterostructure and double-heterostructure diode lasers". IEEE Journal of Quantum Electronics, 11(11):867873, 1975.
- [35] Du, K., et al., "Microfluidic System for Detection of Viral RNA in Blood Using a Barcode Fluorescence Reporter and a Photocleavable Capture Probe", Analytical Chemistry Article ASAP DOI: 10.1021/acs.analchem.7b03527 (2017).
- [36] Ertorer et al., "Femtosecond laser filaments for rapid and flexible writing of fiber Bragg grating", Optics Express 9323 (2017).

- [37] Yin, D., Barber, J.P., Hawkins, A.R, and Schmidt, H., "Waveguide loss optimization in hollow-core ARROW waveguides", *Optics Express*, 13, 9331 (2005).
- [38] Vieu, C., et al. , Electron beam lithography: resolution limits and applications, *Appl. Surf. Sci.*, vol. 164, no.1, pp. 111117, 2000.
- [39] Prinz, V. Y., Grtzmacher, D., Beyer, A., David, C., Ketterer, B., and Deckardt, E., A new technique for fabricating three-dimensional micro- and nanostructures of various shapes, *Nanotechnology*, vol. 12, no. 4, pp. 399402, Dec. 2001.
- [40] Linden, J., Thanner, C., Schaaf, B., Wolff, S., Lgel, B., and Oesterschulze, E., Spray coating of PMMA for pattern transfer via electron beam lithography on surfaces with high topography, *Microelectron. Eng.*, vol. 88, no. 8, pp. 20302032, 2011.
- [41] Zhang, J., Con, C., and Cui, B., Electron Beam Lithography on Irregular Surfaces Using an Evaporated Resist, *ACS Nano*, vol. 8, no. 4, pp. 34833489, Apr. 2014.
- [42] Leech, P. W., Wu, N., and Zhu, Y., Application of dry film resist in the fabrication of microfluidic chips for droplet generation, *J. Micromechanics Microengineering*, vol. 19, no. 6, p. 65019, Jun. 2009.
- [43] Chang, J., et al. (2014), Facile electron-beam lithography technique for irregular and fragile substrates, *Applied Physics Letters*, Volume 105, Issue 17, id.173109
- [44] Jong-Hyun, K., et al., "A Facile Dry-PMMA Transfer process for electron-Beam Lithography on Non-Flat Surfaces". 2017 IEEE 30th International Conference on Micro Electro Mechanical Systems. (2017)

- [45] Schafer, F. P., "Dye lasers. Topics in applied physics". Springer-Verlag, Berlin ; New York, 3rd enl. and rev. edition, 1990.